RSC Advances

REVIEW

View Article Online
View Journal | View Issue

Cite this: *RSC Adv.*, 2025, **15**, 43095

Hydrophobic phenolic/silica aerogel composites with high fire safety and strength for efficient thermal insulation

Zhixin Wang,[a] Yong Kong, *[ab] Mengcheng Nie,[a] Kuo Liu,[c] Qinghua Liu[c] and Xiaodong Shen *[ab]

To develop a polymer-based aerogel composite with excellent fire safety and strength for efficient building insulation, hydrophobic phenolic/silica aerogel composites (PSACs) were synthesized using a facile, self-catalyzed sol–gel process based on co-condensation of resorcinol (R), formaldehyde (F), and 3-(aminopropyl)triethoxysilane (A). The hydrophobicity was achieved *via* the gas-phase modification of the aerogels. The hydrophobicity and thermal conductivity of the PSACs are governed by the R/A ratio and aerogel density, respectively. A glass fiber paper-reinforced PSAC with an R/A ratio of 2 and an aerogel density around 0.10 g cm^{-3} (GP/RA21-10) exhibits a high water contact angle of 138°, a low thermal conductivity of 0.021 W m^{-1} K^{-1}, and a high strength (1.67 MPa of compression strength, 2.54 MPa of tensile strength, and 1.65 MPa of flexural strength). GP/RA21-10 exhibits significantly superior thermal insulation properties compared to commercially available insulation materials, including thermosetting polystyrene board, silica aerogel coating board, and rock wool. GP/RA21-10 is flame-retardant and high-temperature resistant and demonstrates superior fire safety during building insulation. The design presented here offers important guidelines for the advancement of high-performance building insulation materials.

Received 22nd September 2025
Accepted 21st October 2025

DOI: 10.1039/d5ra07166f

rsc.li/rsc-advances

1 Introduction

The consumption of energy and its related carbon emissions during the operation of a building accounted for over 55% of the total building lifecycle emissions, according to the statistics from the China Association of Building Energy Efficiency. Enhancing building thermal insulation performance is a critical measure to reduce carbon emissions during building operation.[1–6] Characterized by their nanoporous structures with high specific surface areas and high nanopore volumes, silica aerogel composites exhibit much lower thermal conductivity than traditional insulation materials such as thermosetting polystyrene board, rock wool, glass wool, and ceramic fiber felt.[7–13] Therefore, silica aerogel composites have been widely applied in many demanding scenarios such as aerospace, electric vehicles, and for energy saving in industrial operations. However, poor mechanical properties limit the application of silica aerogel composites in buildings.[11,14–18]

Polymer aerogels, such as phenolic aerogel, polyimide aerogel, polyurethane aerogel, cellulose aerogel and so on, have better mechanical properties than silica aerogels, and have been studied extensively.[19–32] Phenolic aerogel in particular exhibits both low thermal conductivity and outstanding mechanical performance.[23–32] Pekala *et al.* revealed that phenolic aerogels with densities ranging from 0.1 to 0.2 g cm^{-3} exhibit compressive strengths of 0.1 to 0.2 MPa, much higher than those of silica aerogels (~0.01 MPa).[24] However, phenolic aerogels suffer from poor thermal stability including flammability and poor fire safety.[33] Doping inorganic components into phenolic aerogels is an effective method to enhance their thermal stability and can improve their insulation and mechanical properties significantly.[25–39]

Generally, *in situ* co-polymerization of the phenolic and silica precursors is conducted to develop phenolic/silica composite aerogels with high temperature resistance. Jin *et al.* developed a phenolic/silica aerogel composite, *via* multiple impregnation and ambient pressure drying (APD) steps, from methyltrimethoxysilane (MTMS) and phenolic resin precursors and a quartz fiber reinforcement.[29] The composite had a density of 0.3 g cm^{-3} and a thermal conductivity of 0.044 W m^{-1} K^{-1}. Compared to phenolic aerogel composites without organic components, the addition of silica increased the strength by 40% and reduced the line ablation rate at a heat flux of 0.4 MW m^{-2} by 60%. Wang *et al.* developed a carbon fiber reinforced

[a]College of Materials Science and Engineering, State Key Laboratory of Materials-Oriented Chemical Engineering, Nanjing Tech University, Nanjing 211816, PR China. E-mail: ykong@njtech.edu.cn; xdshen@njtech.edu.cn

[b]Jiangsu Collaborative Innovation Center for Advanced Inorganic Function Composites, Nanjing, 211816, China

[c]Department of Infrastructure, Nanjing Tech University, Nanjing 211816, PR China

phenolic/silica aerogel composite *via* a multi-step sol–gel method and APD, in which the silica solution was dropped into the phenolic solution and stirred at 40 °C until it became homogeneous. Then, the mixed solution underwent a gel-drying process at 80 °C.[30] The resulting aerogel composite exhibited a density of 0.26 g cm^{-3} and a thermal conductivity of 0.055 W m^{-1} K^{-1}. The incorporation of silica led to a 50% enhancement in the maximum fracture strain and a 30% reduction in the line ablation rate under oxyacetylene ablation conditions. Ye *et al.* developed a thermal protection phenolic/silica aerogel *via* a complex sol–gel process and APD, using dimethyldimethoxysilane, MTMS, resorcinol and formaldehyde as precursors, and isocyanate-propyltrimethoxysilane as a coupling agent.[40] The aerogel had a density of 0.12 g cm^{-3} and a thermal conductivity of 0.032 W m^{-1} K^{-1}.

These studies reveal that the thermal stability of phenolic aerogels can be improved by introducing silica. However, the synthesis process is complicated and time-consuming, and the thermal conductivity is still too high for use as high-performance thermal insulation materials. More importantly, the resulting phenolic/silica aerogel composites are hydrophilic, restricting their use in humid environments. In this study, phenolic/silica aerogel composites (PSACs) were developed *via* a facile, self-catalyzed sol–gel process followed by gel drying and aerogel gas-phase modification. The effects of precursor ratio, density, fiber type, and drying method on the architecture and characteristics of the PSACs were explored comprehensively. With low thermal conductivity of 0.021 W m^{-1} K^{-1}, high thermal stability up to 1200 °C, superior hydrophobicity with a water contact angle of 138°, and superior mechanical properties, the PSAC has promise for applications in the domain of building insulation.

2 Experimental

2.1 Materials

Ceramic fiber paper felt (CP, 300 × 300 × 2.50 mm, 0.18 g cm^{-3}) was purchased from Nanjing Gaogeya Fiberglass Development Co., Ltd. Glass fiber paper felt (GP, 300 × 300 × 3.80 mm, 0.16 g cm^{-3}) was purchased from Jiangsu Dali Energy-Saving Technology Co., Ltd. Pre-oxidized PAN fiber needled felt (PANNF, 300 × 300 × 5.00 mm, 0.12 g cm^{-3}) was purchased from Changshu Juge Fiber Products Co., Ltd. Polypropylene fiber felt (PP, 300 × 300 × 5.00 mm, 0.10 g cm^{-3}) was purchased from Xiaoguang Textile Factory. Polyethylene terephthalate felt (PET, 300 × 300 × 5.00 mm, 0.10 g cm^{-3}) was purchased from Guangzhou Hengrui Non-woven Fabric Co., Ltd. Polyethylene felt (PE, 300 × 300 × 1.80 mm, 0.14 g cm^{-3}) was purchased from Hubei Jiateng Textile Co., Ltd. Melamine foam (MF, 300 × 300 × 5.00 mm, 0.05 g cm^{-3}) was purchased from Zhenmo New Material Co., Ltd. 3-(Aminopropyl)triethoxysilane (APTES or A, 98%), formaldehyde (F, 37%), resorcinol (R), and hexamethyldisiloxane (HMDS, 99%) were purchased from Shanghai Aladdin Biochemical Technology Co., Ltd. Ethanol (EtOH, 99.7%) and deionized water (W) were purchased from Nanjing Wanqing Chemical Glassware and Instrument Co., Ltd. All the chemicals were used as received without further purification.

Several commercial insulation materials were used as control samples. Thermosetting polystyrene board (TPSB, 0.20 g cm^{-3}) and extruded polystyrene board (XPSB, 0.04 g cm^{-3}, 0.034 W m^{-1} K^{-1}) were purchased from Xinye Building Materials Business Department. Silica aerogel coating board (SACB, 0.13 g cm^{-3}) was purchased from Shanghai Zhongnan Building Materials Co., Ltd. Rock wool (RW, 0.08 g cm^{-3}) was purchased from Xinlexiang Energy-saving Technology (Shanghai) Co., Ltd.

2.2 Synthesis of hydrophobic PSACs

The synthesis procedure is illustrated in Fig. 1a. R, F, EtOH, and W were combined in a beaker at room temperature with agitation until the R was fully dissolved. APTES was subsequently added to the mixture and stirred for 10 min to prepare the phenolic/silica solution. The fiber felts were impregnated with the phenolic/silica solution with an equal volume. After gelation at 60 °C for 24 h, the wet gels were submerged in ethanol for 48 h to conduct solvent exchange. The alcogels were dried by supercritical drying (SCD) or APD to obtain the PSACs. The hydrophobic modification of the PSACs was conducted using a gas-phase modification at 110 °C for 10 h in a vessel filled with HMDS vapor. As shown in Table S1, PSACs with different R/A molar ratios and densities were prepared, denoted as Z/RA*X*-*Y*, where *X* is the molar ratio of R/A, *Y* is the theoretical density of the pure aerogel (ρ_t), and Z is the type of fiber felt.

2.3 Characterization

The apparent density of the PSACs (ρ_{ac}) was computed based on the weights and physical dimensions of five subsamples. The theoretical density of the pure aerogel (ρ_t) was calculated by assuming that all the reagents react with each other in stoichiometric ratios (eqn (S1)). The chemical architecture was characterized using Fourier-transform infrared spectroscopy (IR-Sprit). The hydrophobic performance was tested using a water contact angle instrument (MIT-100S). The microstructure was observed using scanning electron microscopy (Regulus 8100). The mechanical properties (compressive, tensile, and flexural) were tested with CMT-4204 at a loading rate of 2 mm min^{-1}. The pore structure was characterized on a Belsorp mini X porosimeter. The thermal conductivity (at 25 °C) was tested with a plate heat flow method using an HFM446. Five subsamples of each sample were tested, and the results were averaged. Thermal insulation performance was measured by a back temperature test at a heat source temperature of 70 °C, which was performed using a constant temperature machine (BILON-W-1009S). The flame-retardant performance was examined by using a butane torch flame for a period of 4 minutes and by combusting on an alcohol lamp for 30 s. The weather resistance was tested by outdoor exposure and under a constant environment of 85 °C and 85% relative humidity (BPS-100CH). The building insulation application was tested using heating tapes with the same outside surface temperature (70 °C).

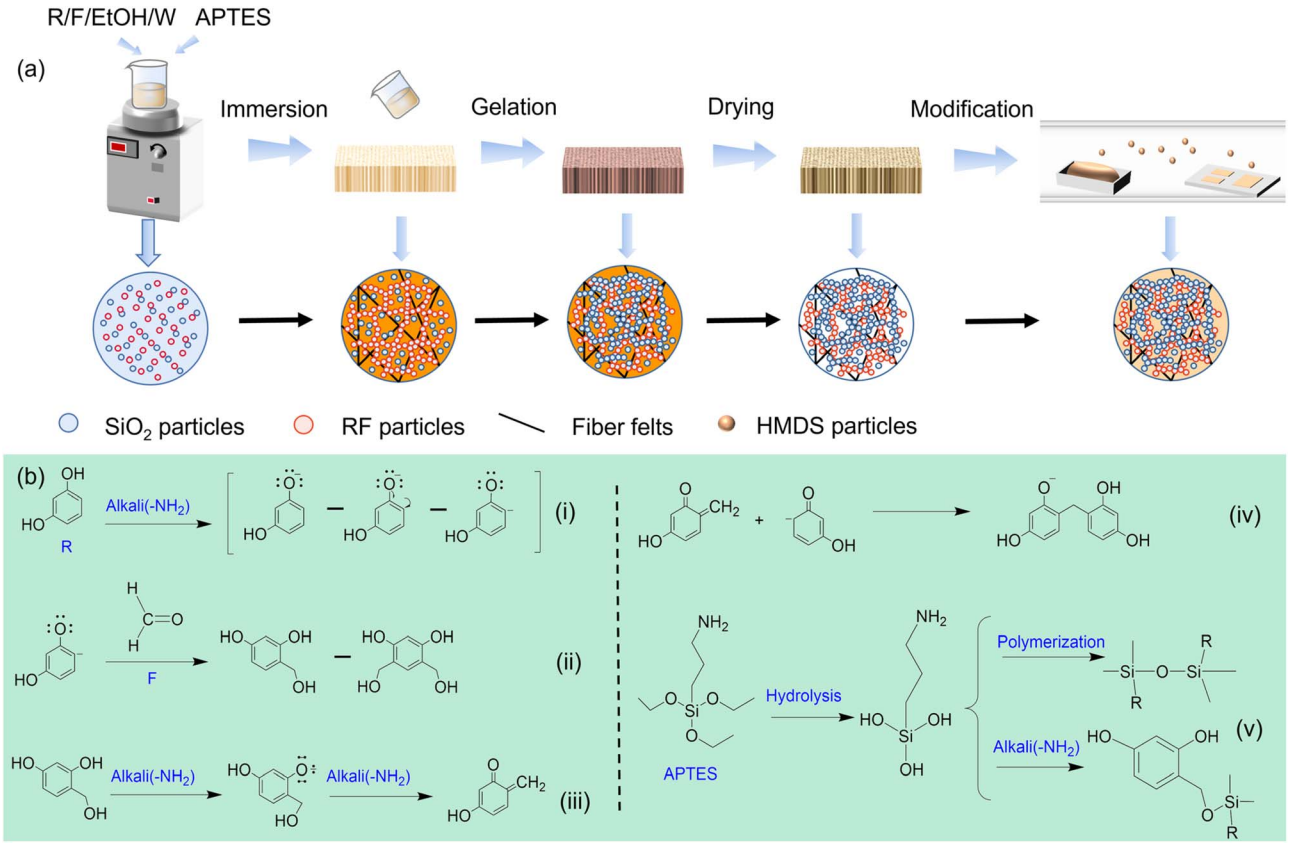

Fig. 1 (a) Preparation of the hydrophobic PSACs and (b) reaction mechanisms that occur during the sol–gel process.

3 Results and discussion

3.1 Sol–gel reaction mechanisms

It is widely recognized that traditional silica aerogels are synthesized *via* a multi-step sol–gel process based on the catalysis of acids and bases.[7–9] In a solution of R/F/A/EtOH/W, a gel can be formed without adding an acid or base catalyst owing to the Lewis base moieties ($-NH_2$) in the APTES.[28] The reaction mechanisms that occur during the sol–gel processes used to make the PSACs are shown in Fig. 1b. The polymerization of R and F is a reaction catalyzed by a Lewis base. First, an R anion is formed through deprotonation Fig. 1b(i). Then, an increase in electron density at the 4 or 6 position of R leads to the hydroxymethylation of the positively charged hydroxyl carbon on F (forming a $-CH_2OH$ group) Fig. 1b(ii). The base catalyst will cause R to generate highly active intermediates (*o*-quinone methyl ether) Fig. 1b(iii), which can react with another molecule of R to form stable methylene bonds Fig. 1b(iv).[41,42] APTES is hydrolyzed to form a Si–OH species, which forms Si–O–Si structures by dehydration condensation. In addition, the Si–OH groups can react with hydroxymethylated R to form Si–O–C linkages Fig. 1b(v).[43,44] The phenolic and Si–O–Si frameworks are mutually interpenetrating, forming a phenolic/silica network with organic and inorganic moieties uniformly hybridized on a molecular scale.

3.2 Effect of the R/A molar ratio and density on the physical properties of the PSACs

The physical properties of the PSACs with different R/A molar ratios and densities are shown in Table S2. All the samples were prepared with CP as the reinforcement using SCD as the drying method. The tiny difference in thickness between the CP and PSACs verifies that there is no obvious volume shrinkage during the synthesis of the PSACs. The apparent densities of the pure aerogels (ρ_a) are calculated by subtracting the contribution of the fiber felt from the apparent densities of the PSACs (ρ_{ac}). It is noted that the values of ρ_a are higher than those of ρ_t, which is attributed to the fact that the reaction does not reach 100% completion.

The FTIR spectra of the PSACs with different R/A molar ratios and the same theoretical density of pure aerogel (0.10 g cm^{-3}) are shown in Fig. 2a. The chemical structure is hardly affected by the R/A molar ratio. The bands around 1150 cm^{-1} are assigned to the Si–O–Si stretching vibrations.[45,53] The bands at 1600 cm^{-1} could be the result of aromatic C=C vibrations or the bending vibration of the $-NH_2$ groups.[38,46] The bands at 850 cm^{-1} are attributed to the Si–C bonds that arise from the formation of a phenolic/silica hybrid network within the PSACs.[47,48] The bands at 2950, 2930, 1450 and 1250 cm^{-1} are assigned to the C–H stretching and deformation vibrations.[49,54]

At a constant theoretical density of pure aerogel (0.10 g cm^{-3}), the water contact angle of the PSACs initially

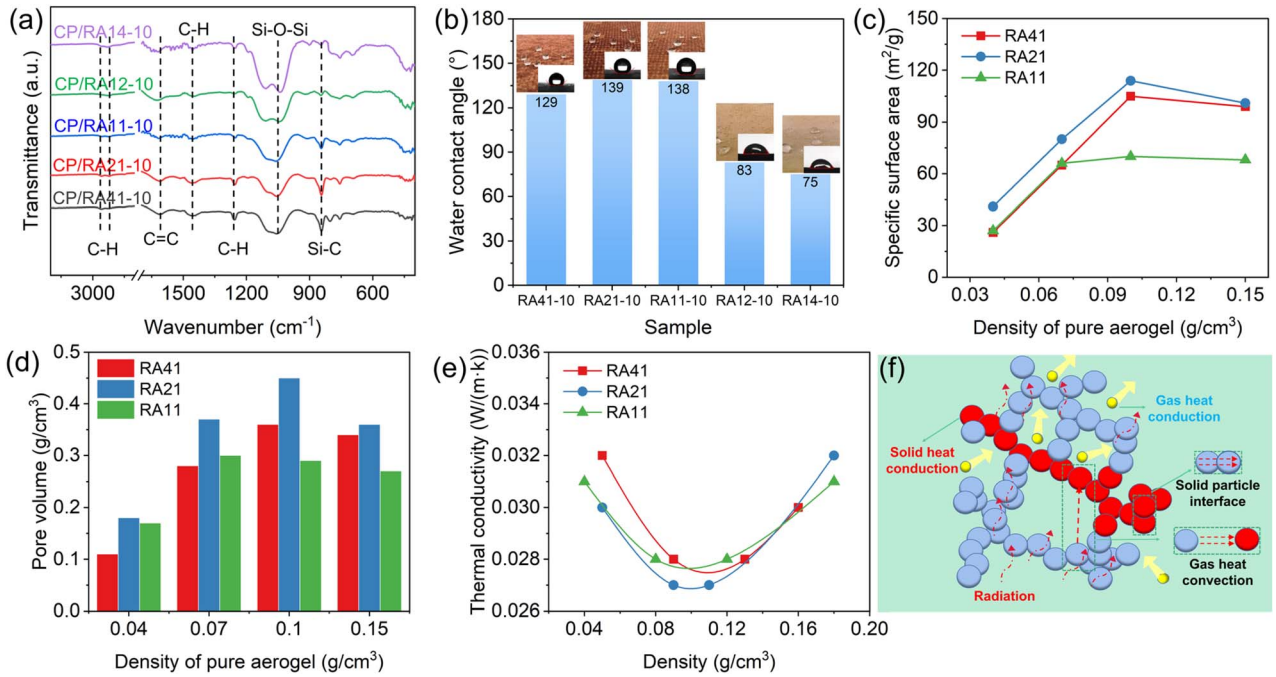

Fig. 2 (a) FTIR spectra of the PSACs with different R/A molar ratios and same theoretical density; (b) water contact angles of the PSACs with different R/A molar ratios; (c) specific surface areas of the PSACs; (d) pore volumes of the PSACs; (e) thermal conductivities of the PSACs with different pure aerogel densities; and (f) thermal insulation mechanism of the PSACs.

increases as the APTES content increases, before starting to decrease as the APTES content continues to rise (Fig. 2b). The highest water contact angle achieved by CP/RA21-10 is 139°. The hydrophobicity is achieved by grafting HMDS on Si–OH species that derive from APTES. However, the APTES contains a strong hydrophilic aminopropyl group. Therefore, the highest water contact angle is obtained with a moderate R/A ratio of 2 : 1. To ensure good hydrophobicity of the PSACs, the R/A molar ratio should not be lower than 1. The influence of the density on the water contact angle of PSACs is weak (Fig. S1).

The pore structure features in the PSACs with different R/A molar ratios and densities are shown in Fig. S2. All samples show type IV isotherms and H2 hysteresis loops without a saturation plateau, indicating the presence of features relating to meso–macroporosity. There is no obvious difference in pore size distribution for the different PSAC samples, and all exhibit a wide pore size distribution in the range of 1–100 nm. It is noted that most pores concentrate in the range of 10–50 nm. The specific surface areas and pore volumes are shown in Fig. 2c and d. The highest specific surface area and pore volume are achieved with a moderate density of 0.10 g cm^{-3}, irrespective of the R/A molar ratio. This is because both higher and lower densities lead to more faults in terms of large voids. For the same theoretical density, a moderate R/A molar ratio of 2 : 1 leads to the highest specific surface area (114 m^2 g^{-1}) and pore volume (0.45 cm^3 g^{-1}).

The relationship between the thermal conductivity (25 °C) and apparent density of the pure aerogel in the PSACs is shown in Fig. 2e. For the PSACs with different R/A molar ratios, all the lowest thermal conductivities are obtained with a moderate density of around 0.10 g cm^{-3} as it leads to the highest specific surface area and pore volume. The PSAC with a R/A molar ratio of 2 exhibits the lowest thermal conductivity of 0.027 W m^{-1} K^{-1}. This is understandable when the thermal transfer mechanism of the aerogel is considered (Fig. 2f). The thermal transfer is mainly composed of solid thermal conduction, gas thermal conduction, gas thermal convection, and thermal radiation. At constant temperature, the effect of gas thermal conduction and thermal radiation is negligible. The solid thermal conduction is suppressed by reducing the contact area of the nanoparticles in the solid framework, or rather by improving the specific surface area. Gas thermal convection can be restrained by reducing the number of macropores and large voids, or rather by improving the pore volume, as determined *via* a N_2 adsorption test.

3.3 Effect of the fiber felt and drying method on the physical properties of the PSACs

Fiber reinforcement has an important influence on the mechanical properties, insulation performance and thermal stability. Seven fiber felts including CP, GP, PANNF, PP, PET, PE and MF were selected for use in the preparation of the PSACs, and the aerogels were prepared with a R/A molar ratio of 2 and a theoretical pure aerogel density of 0.10 g cm^{-3} (RA21-10). Photographs of the PSACs prepared with different reinforcement materials and using different drying methods are shown in Fig. 3a and b. The PSACs made using SCD exhibit an intact and smooth morphology. However, APD leads to obvious volume shrinkage and deformation, especially for the PSAC that has soft MF as a reinforcement material. Consequently, the densities of the PSACs fabricated using APD are higher than those prepared using SCD (Fig. 3c). Moreover, the thermal conductivities of the PSACs synthesized using APD are much

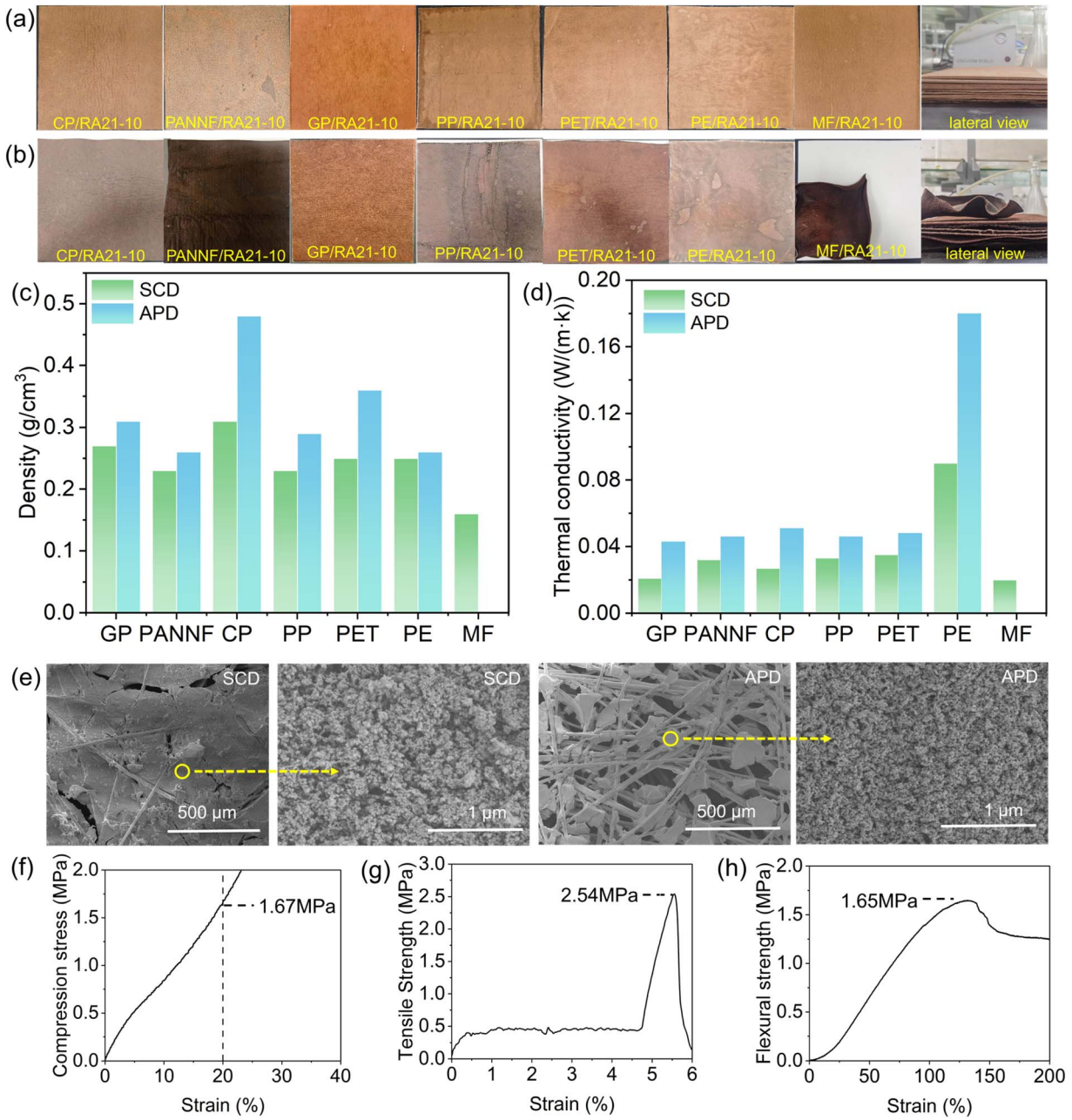

Fig. 3 (a and b) Photographs of PSACs made with different reinforcement materials under (a) SCD and (b) APD; (c) apparent densities of the PSACs made with different reinforcement materials and drying methods; (d) thermal conductivities of the PSACs made with different reinforcement materials and drying methods; (e) SEM images of GP/RA21-10 made using SCD and APD; and (f–h) stress–strain curves of GP/RA21-10: (f) compressive; (g) tensile; and (h) flexural.

higher than those of the PSACs prepared using SCD (Fig. 3d). This finding is attributed to the generation of large voids and the aggregation of nanoparticles during APD, which result from the damage to the porous structure caused by capillary force (Fig. 3e and S3). These findings indicate that SCD is necessary to obtain high-performance PSACs for thermal insulation.

During SCD, the thermal conductivities of the PSACs reinforced with different fiber reinforcement materials including GP, CP, PANNF, PP, PET, PE and MF are 0.021, 0.027, 0.032, 0.033, 0.035, 0.090 and 0.020 $W\,m^{-1}\,K^{-1}$, respectively. The effect of reinforcement on thermal conductivity is attributed to the microstructure of the reinforcement materials, as shown in Fig. S4. CP, PANNF, PP, PE and PET exhibit disorderly and close stacking of their fibers. However, MF and GP exhibit uniform porous frameworks with fine skeletons or fibers. The uniform microstructure favors the impregnation of phenolic/silica sol and the suppression of solid thermal conduction. Hence, the PSACs reinforced with GP and MF (GP/RA21-10 and MF/RA21-10) exhibit lower thermal conductivity than the other samples. However, the hydrophobicity of the PSACs is hardly affected by the fiber type (Fig. S5). It should be noted that MF/RA21-10 is flammable and is not suitable for thermal insulation in

buildings. GP/RA21-10 is optimal for insulation in buildings. Furthermore, GP/RA21-10 exhibits much higher compression strength than the other PSAC samples (Fig. S6). The Young's modulus of GP/RA21-10 is 65.3 MPa, and the compression strength is 1.67 MPa at 20% strain (Fig. 3f). As shown in Fig. 3g, the tensile strength of GP/RA21-10 is 2.54 MPa with a failure strain of 5.5%. Fig. 3h demonstrates that GP/RA21-10 has high bending deformation, and the failure bending strain and strength are 105% and 1.65 MPa, respectively. The strength of GP/RA21-10 is much higher than typical silica aerogel composites, which exhibit a compression strength of 0.18 MPa.[50,51]

3.4 Thermal insulation performance

The thermal conductivity of GP/RA21-10 and its state-of-the-art counterparts including other reported polymer/silica aerogels and commercial insulation materials are shown in Fig. 4a. GP/RA21-10 has a much lower thermal conductivity than other phenolic/silica aerogel composites (OPSACs),[30,31,52] a polyimide/silica aerogel composite (PISAC),[22] a polyvinyl alcohol/silica aerogel composite (PVASAC),[11] and commercial insulation materials including TPSB, SACB, and RW.

The insulation performance under practical building insulation conditions is determined on a hot plate apparatus (Fig. 4b). With thermal insulation materials fixed on a 70 °C plate, the temperatures of the cold side (back temperatures) were collected. The back temperatures of samples of GP/RA21-10, TPSB, SACB and RW with the same thickness (40 mm) are shown in Fig. 4c. After 8 h, the stabilized back temperatures of GP/RA21-10, TPSB, SACB and RW were 27.3, 33.4, 32.3 and 33.0 °C, respectively. To achieve the same insulation performance with a back temperature of 33 ± 1 °C on a hot plate of 70 °C, the thicknesses of GP/RA21-10, TPSB, SACB, and RW required were 20, 40, 40, and 50 mm, respectively (Fig. 4d). The insulation performance of GP/RA21-10 is superior to that of other commercial insulation materials.

3.5 Flame-retardant performance

TPSB is widely used for building insulation in China as it can achieve a fire rating of A2. The flammability of GP/RA21-10 (5 mm) and TPSB (5 mm) was compared by combustion with an

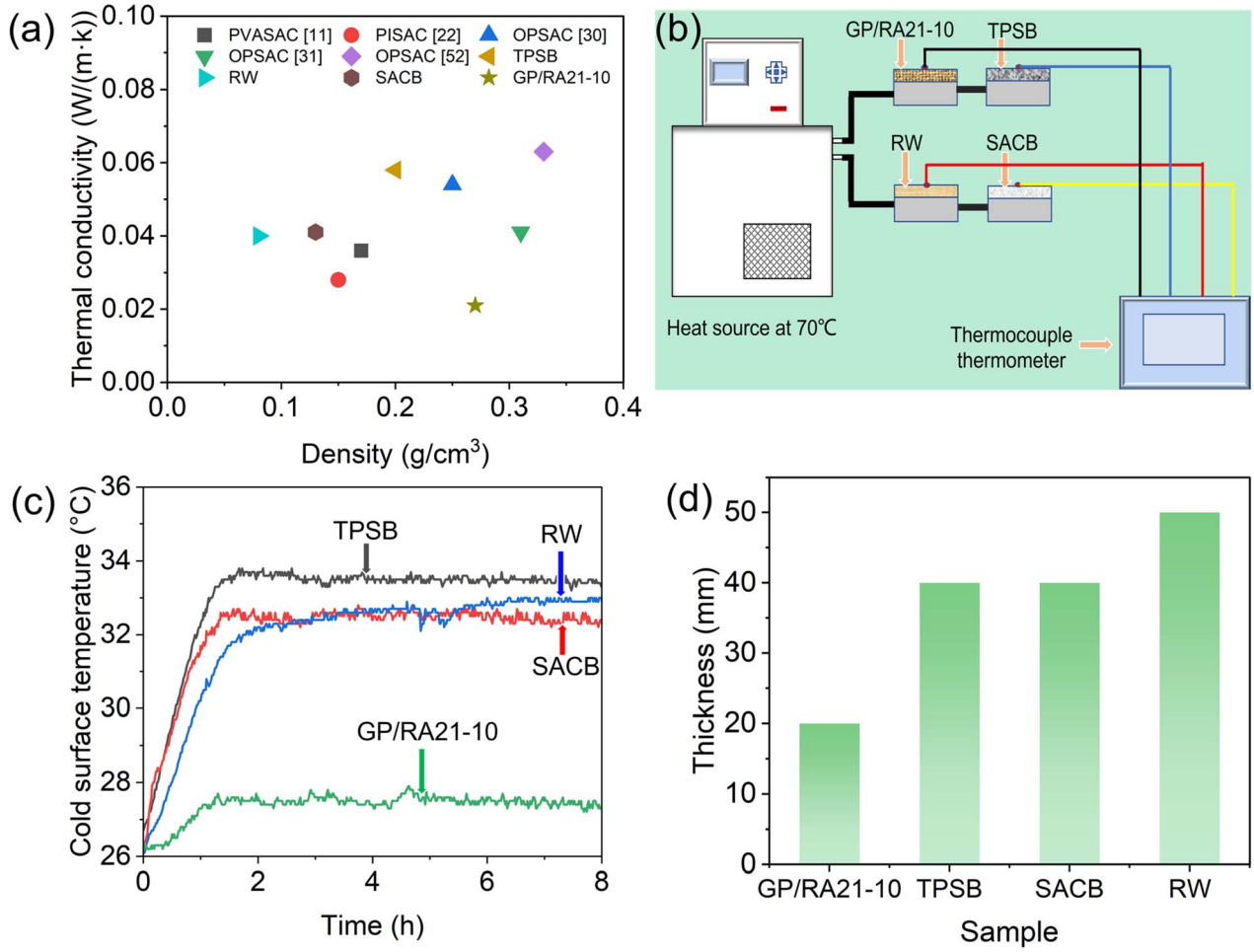

Fig. 4 (a) Thermal conductivities of GP/RA21-10 and its state-of-the-art counterparts (data of the commercial materials were measured together with GP/RA21-10); (b) hot plate apparatus used to estimate the insulation performance; (c) back temperatures of samples of GP/RA21-10, TPSB, SACB, and RW with same thickness (40 mm); and (d) thicknesses of GP/RA21-10, TPSB, SACB, and RW required to achieve same insulation performance with a back temperature of 33 ± 1 °C.

alcohol lamp for 30 s (Fig. 5a, b and Video S1). Both GP/RA21-10 and TPSB are flame-retardant and self-extinguish after removing the flame. However, the polymer component in TPSB is burnt off gradually. The thermal shock resistance of GP/RA21-10 (20 mm) and TPSB (40 mm) was investigated under a butane torch flame with a temperature of up to 1200 °C, and the back temperatures were recorded using a thermocouple (Fig. 5c and Video S2). The back temperatures of GP/RA21-10 and TPSB were 34 and 39 °C at 4 min, respectively. Initially, both GP/RA21-10 and TPSB demonstrated superior insulation performance. However, the insulation performance of TPSB degraded remarkably with time as the polymer component was burnt off (Fig. 5c).

GP/RA21-10, after ablation, is divided into the ablative layer, the carbonized layer and the original material (Fig. 5d). The flame-retardant mechanism of GP/RA21-10 relies on the dual

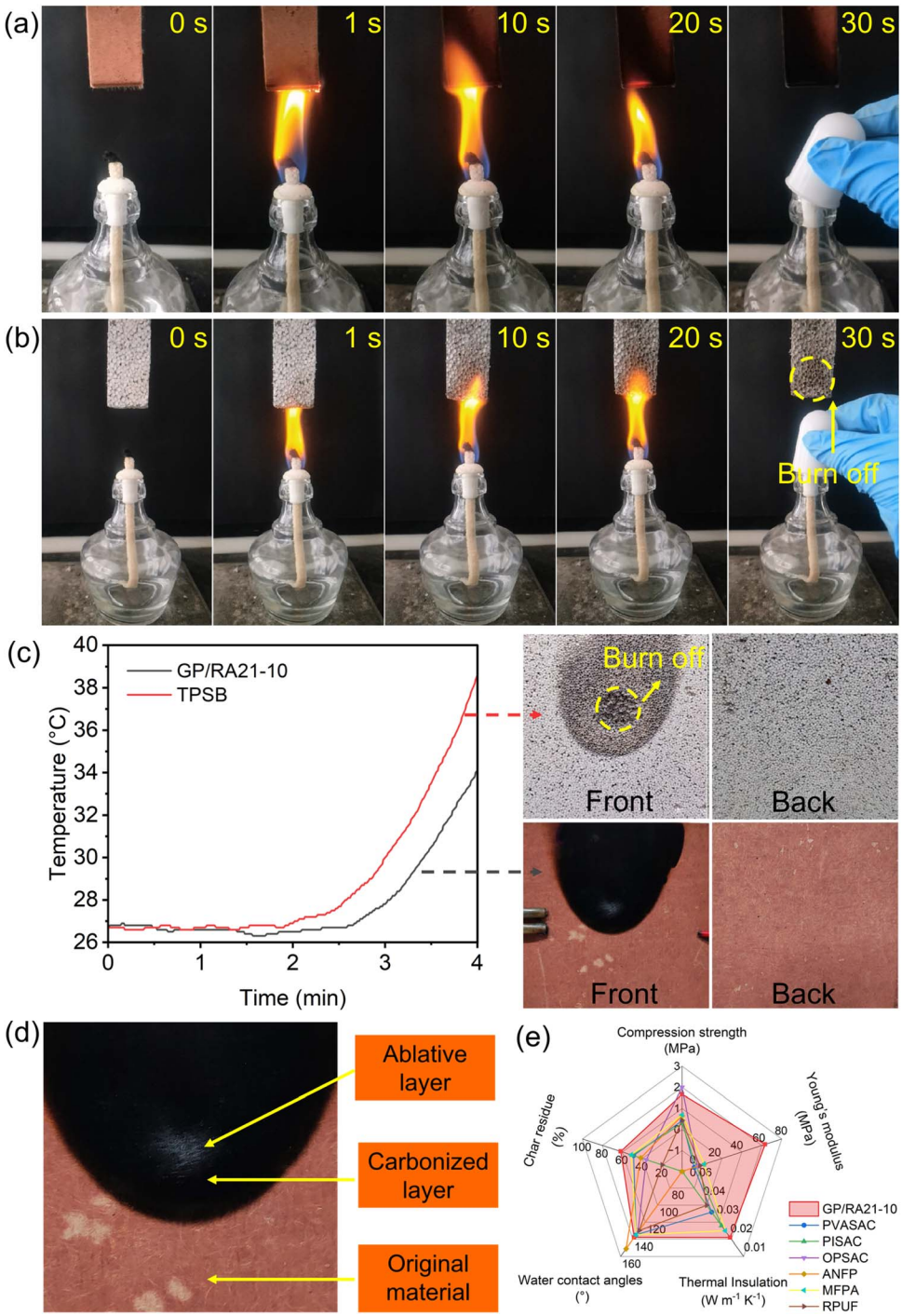

Fig. 5 (a and b) Photographs of GP/RA21-10 (a) and TPSB (b) when subjected to combustion with an alcohol lamp (sample thickness: 5 mm); (c) back temperatures and photographs of GP/RA21-10 (20 mm) and TPSB (40 mm) under a butane torch flame; (d) photograph of GP/RA21-10 after ablation; and (e) comparison of the performance of GP/RA21-10 with other reported insulation aerogels.

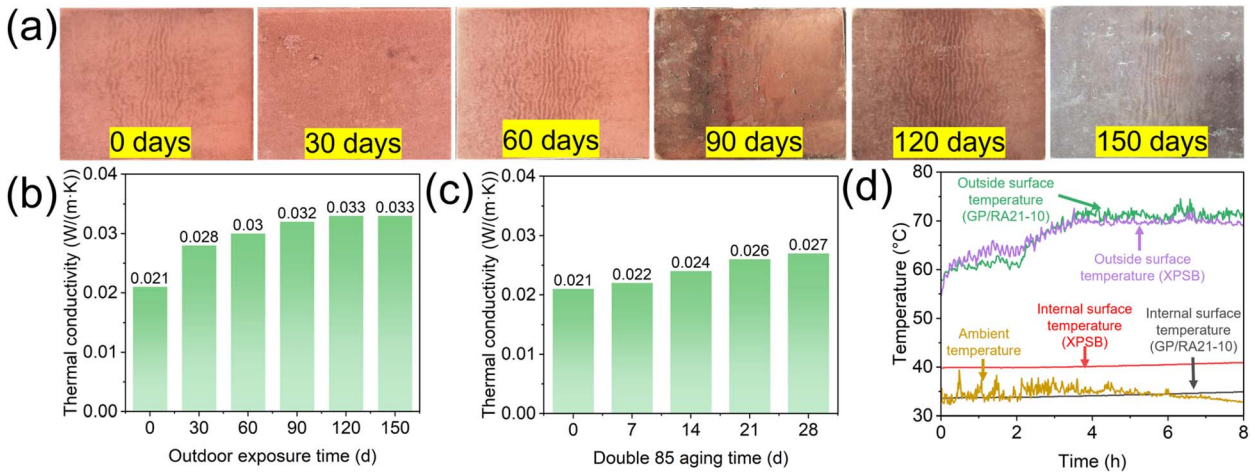

Fig. 6 (a) Photographs of GP/RA21-10 after outdoor exposure for 150 d; (b) thermal conductivities of GP/RA21-10 after outdoor exposure for different time periods; (c) thermal conductivities of GP/RA21-10 after double 85 aging for different time periods; and (d) external building wall insulation performances of GP/RA21-10 and XPSB.

synergy of the organic–inorganic phases and glass fiber-matrix. The pyrolysis of the organic components in the composite takes away most of the heat. Meanwhile, the inorganic components transform into SiO_2 at elevated temperatures, leading to the formation of a dense layer.[26,30] This dense layer adheres to the surface of the aerogel, inhibiting the transfer of heat and oxygen. In addition, the glass fiber skeleton effectively maintains the structural stability of the aerogel, further lessening the impact of the flames and reducing heat transfer, thereby protecting the deeper layers of the base material.[52] Fig. 5e compares the performance of GP/RA-10 and other reported insulation aerogels in terms of compression strength, Young's modulus, thermal insulation, water contact angle and char residue. Details of these properties are included in Table S3. The results indicate that the as-prepared aerogel composite has a better fire safety profile, especially under the effects of a long-term fire atmosphere.

3.6 Weather resistance and application in building insulation

To evaluate the weather resistance of GP/RA21-10, the material was directly placed on the roof to conduct an outdoor exposure test for 150 days (from December to May in Jiangsu, China). The color of GP/RA21-10 darkens gradually within 120 d, and the surface exhibits obvious damage after 150 d (Fig. 6a). This finding is attributed to the decomposition of phenolic components by ultraviolet radiation. The thermal conductivity of GP/RA21-10 increases gradually within 120 d and stabilizes at 0.033 W m^{-1} K^{-1} (Fig. 6b). Alternatively, an accelerated aging test was conducted under constant environmental conditions of 85 °C and 85% relative humidity (double 85 test) to further understand the weather resistance. The thermal conductivities of GP/RA21-10 after double 85 aging for different times are shown in Fig. 6c, and the thermal conductivity gradually increases with aging time due to the moisture-induced damage of the porous structure.

GP/RA21-10 products with a thickness of 20 mm were applied in buildings as external wall insulation materials, and their actual performance was compared with a commercial insulation material, XPSB, with a thickness of 20 mm. When exposed to an outside external wall surface temperature of 70 °C, the internal surface temperature of the GP/RA21-10 insulation material was 6 °C lower than that of XPSB, the insulation material (Fig. 6d). The results indicate that GP/RA21-10 has much better insulation performance than traditional insulation materials.

4 Conclusions

PSACs were synthesized *via* a facile, self-catalyzed sol–gel process followed by drying of the gels and gas-phase modification of the aerogels. The sol–gel reaction occurs *via* the self-catalysis of APTES, leading to a phenolic/silica network with organic and inorganic components hybridized uniformly at the molecular level. To ensure good hydrophobicity of the PSACs, the R/A molar ratio should not be lower than 1, whilst the highest water contact angle is achieved with a moderate R/A molar ratio of 2 : 1. For the PSACs with different R/A molar ratios, the lowest thermal conductivities are obtained with a moderate aerogel density around 0.10 g cm^{-3} as this leads to the highest specific surface area and pore volume. The PSACs made using SCD exhibit a more intact and smoother morphology compared to those made using APD, thus leading to materials with lower density and thermal conductivity. The effect of the fiber reinforcement material on hydrophobicity is minor, but its effect on thermal conductivity is significant. Here, MF and GP with uniform porous frameworks with fine skeletons or fibers lead to low thermal conductivity. However, GP/RA21-10 offers significant advantages in terms of hydrophobicity, fire safety, thermal insulation, and strength, whilst reducing the use of building insulation materials by half and lowering the overall cost. Therefore the MF-based PSAC is

flammable and is not suitable for building insulation. As a result, a GP-reinforced PSAC with an R/A ratio of 2 : 1 and an aerogel density around 0.10 g cm^{-3} (GP/RA21-10) exhibits a high water contact angle of 138° and a low thermal conductivity of 0.021 W m^{-1} K^{-1}. Moreover, GP/RA21-10 has a high compression strength of 1.67 MPa, a tensile strength of 2.54 MPa, and a flexural strength of 1.65 MPa. The thermal conductivity of GP/RA21-10 is much lower than other phenolic/silica aerogel composites, exhibiting significantly superior thermal insulation properties and fire safety compared to commercially available insulation materials, GP/RA21-10 has great promise as an efficient building insulation material.

Author contributions

Zhixin Wang: investigation, data curation, and writing-original draft. Yong Kong: writing-review and editing, methodology, funding acquisition, and administration. Mengcheng Nie: validation and supervision. Kuo Liu: supervision. Qinghua Liu: supervision. Xiaodong Shen: supervision and funding acquisition.

Conflicts of interest

The authors declare that they have no known competing financial interests or personal relationships that could have appeared to influence the work reported in this paper.

Data availability

Data will be made available on request.

Supplementary information is available. See DOI: **https://doi.org/10.1039/d5ra07166f**.

Acknowledgements

The authors acknowledge the financial support from the Program Fund of the Non-Metallic Excellence and Innovation Center for Building Materials (24TDA-2) and the Priority Academic Program Development of Jiangsu Higher Education Institution (PAPD).

References

1 X. Jiang, Y. Kong, Z. Y. Zhao and X. D. Shen, Spherical amine grafted silica aerogels for CO_2 capture, *RSC Adv.*, 2020, **10**(43), 25911–25917.
2 M. Di Luigi, Z. P. Guo, L. An, J. N. Armstrong, C. Zhou and S. Q. Ren, Manufacturing silica aerogel and cryogel through ambient pressure and freeze drying, *RSC Adv.*, 2022, **12**(33), 21213–21222.
3 Y. J. Dai, Y. Q. He, D. D. Yu, J. B. Dai, Y. G. Wang and F. Bai, Study on the effect of semi-transparency on thermal insulation performance of silica aerogel composites, *Case Stud. Therm. Eng.*, 2024, **54**, 104010.
4 Q. An, M. Bagheritabar, A. Basem, A. A. Ghabra, Y. Q. Li, M. Tang, L. S. Sabri and R. Sabetvand, The effect of size of copper oxide nanoparticles on the thermal behavior of silica aerogel/paraffin nanostructure in a duct using molecular dynamics simulation, *Case Stud. Therm. Eng.*, 2024, **60**, 104666.
5 S. B. Jadhav, A. Makki, D. Hajjar and P. B. Sarawade, Synthesis of light weight recron fiber-reinforced sodium silicate based silica aerogel blankets at an ambient pressure, *J. Porous Mater.*, 2022, **29**, 957–969.
6 S. Jadhav and P. Sarawade, Recent advances and prospective of reinforced silica aerogel nanocomposites and their applications, *Eur. Polym. J.*, 2024, **206**, 112766T.
7 T. Zhang, D. P. Yu, F. H. Xu, Y. Kong and X. D. Shen, Flexible silica aerogel composites for thermal insulation under high-temperature and thermal-force coupling conditions, *ACS Appl. Nano Mater.*, 2024, **7**(6), 6326–6338.
8 D. P. Yu, M. Liu, F. H. Xu, Y. Kong and X. D. Shen, Structure tailoring and thermal performances of water glass-derived silica aerogel composite with high specific surface area and enhanced thermal stability, *J. Non-Cryst. Solids*, 2024, **630**, 122889.
9 Q. Liu, W. J. Zhu, Y. Kong, C. Chu and X. D. Shen, New insights into the resistance of hydrophobic silica aerogel composite to water, moisture, temperature and heat-stress coupling, *Ceram. Int.*, 2024, **50**(20), 38189–38199.
10 Q. Liu, Y. Kong, Z. Q. Sun, Z. Y. Liu and X. D. Shen, Facile synthesis of amine hybrid silica aerogel globule via wet casting assisted self-catalysed sol-gel process for CO_2 capture including direct air capture, *J. Environ. Chem. Eng.*, 2024, **12**(3), 112913.
11 D. Duan, X. D. Gao, Y. B. Dong, X. M. Qi, X. X. Zhang, M. D. Z. Islam, Y. Q. Wu, X. Zhao and X. M. Li, Green preparation of thermal-insulative, flame retardant, and hydrophobic silica aerogel reinforced poly(vinyl alcohol) composites, *ACS Appl. Polym. Mater.*, 2022, **4**(10), 7352–7362.
12 M. Liu, Y. L. Huang, C. Xu, S. J. Yao, G. X. Long, Q. Liu, C. G. Fang and X. X. Wu, Realizing balanced thermal safety and heat insulation in hydrophobic silica aerogel composites, *Polym. Degrad. Stab.*, 2025, **236**, 111294.
13 G. Marceau, L. Bertrand and C. Jean-Philippe, Insulation materials for building: dealing with climate change along with other challenges yet to come, *IOP Conf. Ser. Earth Environ. Sci.*, 2024, **1402**(1), 012052.
14 Y. H. Wang, X. N. Luo, Q. Li, W. L. Wang, Q. L. Du, H. Yang, L. J. Qiu, Z. Zhang and J. Shen, Industrial application of SiO_2 aerogel prepared by supercritical ethanol (SCE) drying technique as cold and heat insulation materials, *J. Sol-Gel Sci. Technol.*, 2023, **106**(2), 341–348.
15 J. Ren, Z. Y. Zhao, Y. Kong, K. M. Zhu, W. Jiang, M. Yuan, J. Q. Tang and X. D. Shen, General approach to the synthesis of metal hybrid carbon/titania aerogel for the oxygen reduction reaction, *Energy Fuels*, 2024, **38**(9), 8262–8276.
16 Q. Liu, Y. Kong and X. D. Shen, Regulating the hydrophobicity and pore structure of silica aerogel for thermal insulation under humid and high temperature conditions, *J. Porous Mater.*, 2024, **32**(1), 171–180.

17 M. Liu, Y. Kong, B. Q. Zhang and X. D. Shen, New insights into the resistance of silica aerogel to temperature up to 1200 °C, *Mater. Lett.*, 2024, **372**, 13705.

18 J. Tang, H. W. Sang, J. H. Chen, H. H. Min, X. Y. Wu, W. D. Zang, J. C. Liu, X. M. Liu, Y. Kong, X. D. Shen, H. Yang, Y. Q. Bu and H. H. Zhang, The use of thin aerogel sheets to suppress the thermal runaway propagation of high energy density cells ($LiNi_{0.8}Co_{0.1}Mn_{0.1}O_2$/Si-C) based module, *Process Saf. Environ. Prot.*, 2024, **186**, 1087–1096.

19 X. Y. Zhao, F. Yang, Z. C. Wang, P. M. Ma, W. F. Dong, H. Q. Hou, W. Fan and T. X. Liu, Mechanically strong and thermally insulating polyimide aerogels by homogeneity reinforcement of electrospun nanofibers, *Composites, Part B*, 2020, **182**, 107624.

20 H. Wang, M. Cao, H. B. Zhao, J. X. Liu, C. Z. Geng and Y. Z. Wang, Double-cross-linked aerogels towards ultrahigh mechanical properties and thermal insulation at extreme environment, *Chem. Eng. J.*, 2020, **399**, 125698.

21 J. Y. Xue, R. N. Han, Y. M. Li, J. X. Zhang, J. X. Liu and Y. Yang, Advances in multiple reinforcement strategies and applications for silica aerogel, *J. Mater. Sci.*, 2023, **58**(36), 14255–14283.

22 Z. F. Fei, Z. C. Yang, G. B. Chen, K. F. Li, S. Zhao and G. H. Su, Preparation and characterization of glass fiber/polyimide/SiO_2 composite aerogels with high specific surface area, *J. Mater. Sci.*, 2018, **53**, 12885–12893.

23 C. F. Yuan, D. G. Wang, Y. J. Zhang, K. Li and J. Ding, Research progress on preparation, modification, and application of phenolic aerogel, *Nanotechnol. Rev.*, 2023, **12**(1), 39.

24 R. W. Pekala and J. D. LeMay, Organic aerogels: microstructural dependence of mechanical properties in compression, *J. Non-Cryst. Solids*, 1990, **125**, 67–75.

25 T. Liu, W. H. Jiang, H. Q. Qian, X. R. Shi, J. X. Chen, Q. Y. Cao, N. Li, Y. D. Huang and B. Jiang, Nitrogen-Coordinated borate esters induced entangled heterointerface toward multifunctional silicone/phenolic binary aerogel composites, *Chem. Eng. J.*, 2024, **482**, 149061.

26 C. Wu, L. M. Wang, X. J. Yan, H. Huang, Y. W. Pan, H. B. Wang, W. Wang, S. Yuan, J. H. Fan, X. Y. Jin, C. Q. Hong and X. H. Zhang, Environmental-friendly and fast production of ultra-strong phenolic aerogel composite with superior thermal insulation and ablative-resistance, *Compos. Sci. Technol.*, 2024, **256**, 110776.

27 H. D. Fu, Y. Qin, Z. W. Peng, J. P. Dou and Z. X. Huang, A novel co-continuous Si-Zr hybrid phenolic aerogel composite with excellent antioxidant ablation enabled by sea-island-like ceramic structure at high temperature, *Ceram. Int.*, 2024, **50**(12), 21008–21019.

28 J. Ren, T. Zhang, Y. Kong, Z. Y. Zhao, K. M. Zhu, X. Q. Zhang and X. D. Shen, Facile synthesis of phenolic-reinforced silica aerogel composites for thermal insulation under thermal-force coupling conditions, *Ceram. Int.*, 2023, **49**(18), 29820–29828.

29 X. Y. Jin, J. G. Xu, Y. W. Pan, H. B. Wang, B. Ma, F. Liu, X. J. Yan, C. Wu, H. Huang, H. M. Cheng, C. Q. Hong and X. H. Zhang, Lightweight and multiscale needle quartz fiber felt reinforced silicon oxycarbide modified phenolic aerogel nanocomposite with enhanced mechanical, insulative and flame-resistant properties, *Compos. Sci. Technol.*, 2021, **217**, 109100.

30 W. K. Wang, W. J. Xu, X. F. Jia, F. H. Zhang, Y. P. Cao, C. Ma, J. T. Wang, W. M. Qiao and L. C. Ling, A facile in-situ strategy to fabricate lightweight carbon fiber/silicone-phenolic aerogel composites with superior toughness and ablation performance, *J. Mater. Sci.*, 2024, **59**(39), 18488–18498.

31 R. X. Liu, H. B. Wang, C. Q. Hong, X. Y. Jin, Y. W. Pan and X. H. Zhang, Mechanical and dual-stage wind tunnel ablative behavior of ceramic fiber-tile reinforced phenolic aerogel, *Compos. Commun.*, 2022, **36**, 101386.

32 L. Wang, X. M. Hu, R. Huang, M. T. Huang, X. Liu, Z. M. Zhou, P. J. Guo, Z. L. Mao, X. S. Xu and X. Wang, Elastic, antiflaming phenolic aerogels for advanced thermal protection at extreme environments, *Compos. Commun.*, 2024, **48**, 101889.

33 H. B. Wang, X. J. Yan, X. Y. Jin, Y. W. Pan, C. Wu, H. Huang, C. Q. Hong and X. H. Zhang, Mechanical and thermal ablative behavior of ceramic-modified lightweight quartz felt reinforced phenolic aerogel, *Compos. Commun.*, 2022, **35**, 101285.

34 Q. You, G. Liu, Y. Zhong, H. H. Xu, X. F. Zhang, S. S. Shang, M. Yuan, S. Cui and X. D. Shen, Mechanical properties and oxidative ablation behaviors of polysilazane-modified phenolic resin aerogel/carbon fiber fabric composites, *Polym. Compos.*, 2023, **45**(1), 1.

35 H. Huang, Y. H. Lv, X. Y. Jin, H. B. Wang, C. Wu, Y. W. Pan, X. J. Yan, C. Q. Hong, W. B. Han and X. H. Zhang, Bifunctional silicone triggered long-range crosslinking phenolic aerogels with flexibility and thermal insulation for thermal regulation, *Chem. Eng. J.*, 2023, **470**, 144413.

36 F. Z. Li, J. B. Song, Y. T. Niu, H. W. Zhang, M. Niederberger and W. Cheng, Superelastic cobalt silicate@resorcinol formaldehyde resin core-shell nanobelt aerogel monoliths with outstanding fire retardant and thermal insulating capability, *Small*, 2023, **19**(50), e2302724.

37 Y. L. Cheng, J. W. Zhang, C. Ren, S. P. Zhao, X. D. Zhang and J. P. Fan, Facile preparation of high-strength SiC/C aerogels from pre-reacted resorcinol-formaldehyde and siloxane, *J. Ind. Eng. Chem.*, 2023, **134**, 75–83.

38 F. H. Xu, Y. X. Wang, F. C. Tang, X. L. Dai, Z. Y. Zhao, Y. Kong, X. D. Shen and G. F. Shao, Synergistic enhancement of structure and function in carbonaceous SiC aerogels for improved microwave absorption, *Carbon*, 2025, **233**, 119854.

39 X. Y. Jin, C. Liu, H. Huang, R. Q. Pan, C. Wu, X. J. Yan, H. B. Wang, Y. W. Pan, C. Q. Hong and X. H. Zhang, Multiscale, elastic, and low-density carbon fibre/silicon oxycarbide-phenolic interpenetrating aerogel nanocomposite for ablative thermal protection, *Composites, Part B*, 2022, **245**, 110212.

40 D. N. Ye, H. L. Lv, Z. R. Zheng and L. J. Luo, Preparation and properties of flexible phenolic silicone hybrid aerogels for thermal insulation, *Molecules*, 2024, **29**(20), 4942.

41 Y. Kong, J. Y. Zhang, Z. Y. Zhao, X. Jiang and X. D. Shen, Monolithic silicon nitride-based aerogels with large specific surface area and low thermal conductivity, *Ceram. Int.*, 2019, **45**(13), 16331–16337.

42 Y. Kong, J. Y. Zhang and X. D. Shen, One-pot sol–gel synthesis of amine hybrid titania/silsesquioxane composite aerogel for CO_2 capture, *J. Sol-Gel Sci. Technol.*, 2017, **84**(3), 422–431.

43 B. F. Sandrine, H. Claudia, I. Pierre, J. Edward and T. Salvatore, Evaluation of lightweight and flexible insulating aerogel blankets based on resorcinol-formaldehyde-silica for space applications, *Eur. Polym. J.*, 2017, **93**, 403–416.

44 B. X. Liu, W. Ju, J. Zhang, H. L. Fan, Q. C. Wang, X. B. Yi, Z. C. Yu and X. Q. Wang, Improvement of mechanical strength of ultralight resorcinol-formaldehyde/silica aerogel by addition of zirconia, *J. Sol-Gel Sci. Technol.*, 2017, **83**(1), 100–108.

45 J. Yan, M. X. Kuang, Y. L. Zhu, Y. K. Chen, C. H. Zhang, H. L. Ma, X. Q. Zhang and L. Kong, Facile, tunable, and environmental friendly synthesis of silica/resorcinol-formaldehyde hybrid xerogels with ultra-low shrinkage using a cationic polyelectrolyte as a soft template, *J. Porous Mater.*, 2023, **30**(1), 103–113.

46 Z. Y. Zhao, Y. Cui, Y. Kong, J. Ren, X. Jiang, W. Q. Yan, M. Y. Li, J. Q. Tang, X. Q. Liu and X. D. Shen, Thermal and mechanical performances of the superflexible, hydrophobic, silica-based aerogel for thermal insulation at ultralow temperature, *ACS Appl. Mater. Interfaces*, 2021, **13**(18), 21286–21298.

47 B. L. Shi, Z. L. Zhou, Y. Chen, X. Q. Wang and B. S. Xu, Preparation and properties of hydrophobic and highly transparent SiO_2 aerogels, *Ceram. Int.*, 2023, **49**(16), 27597–27603.

48 H. K. Zhao, H. Y. Wang, L. Chen, L. L. Wang and X. Zhao, Preparation of low-cost silica aerogels by high-pressure carbon dioxide methods, *J. Non-Cryst. Solids*, 2025, **656**, 123474.

49 J. Wei, X. T. Li, Y. Wang, B. Chen, M. J. Zhang and C. M. Qin, Photoluminescence property of inexpensive flexible SiC nanowires membrane by electrospinning and carbothermal reduction, *J. Am. Ceram. Soc.*, 2020, **103**(11), 6187–6197.

50 J. Y. Xue, L. P. Liu, Y. L. Meng, Z. Chen and Y. Yang, Constructing powerful interface between glass fiber and silica aerogel via an interfacial molecular bridge allows for excellent acoustic-thermal insulation composites, *Constr. Build. Mater.*, 2025, **465**, 140260.

51 E. Haq, S. F. A. Zaidi, M. Zubair, M. R. A. Karim, S. K. Padmanabhan and A. Licciulli, Hydrophobic silica aerogel glass-fibre composite with higher strength and thermal insulation based on methyltrimethoxysilane (MTMS) precursor, *Energy Build.*, 2017, **151**(1), 494–500.

52 X. Y. Jin, C. Wu, H. B. Wang, Y. W. Pan, H. Huang, W. Wang, J. H. Fan, X. J. Yan, C. Q. Hong and X. H. Zhang, Synergistic reinforcement and multiscaled design of lightweight heat protection and insulation integrated composite with outstanding high-temperature resistance up to 2500 °C, *Compos. Sci. Technol.*, 2023, **232**, 109878.

53 F. H. Y, P. F. Jia, L. Song, Y. Hu, B. B. Wang and R. Y. Wu, Multifunctional fabrics based on copper sulfide with excellent electromagnetic interference shielding performance for medical electronics and physical therapy, *Chem. Eng. J.*, 2023, **472**, 145091.

54 F. H. Yu, P. F. Jia, B. B. Wang, L. Song and Y. Hu, Unlocking a dual-mode thermal regulation and electromagnetic protection strategy under extreme conditions via bidirectional Janus design, *J. Mater. Chem. A*, 2025, **13**, 23547.